Multilayer assembly of thin-film nanocomposite membranes with enhanced NaCl and antibiotic rejection

Pengcheng Su,[a#] Miaomiao Jia,[a#] Junping Huang,[a] Wanbin Li, [a,b,*] and Chuyang Y. Tang[b,*]

[a] Guangdong Key Laboratory of Environmental Pollution and Health, School of Environment, Jinan University, Guangzhou 511443, P.R. China.

[b] Department of Civil Engineering, The University of Hong Kong, Pokfulam, Hong Kong 999077, P. R. China.

*Corresponding authors: E-mail: gandeylin@126.com (W. Li), tangc@hku.hk (C. Tang)

[#]These authors contributed equally to this work.

ABSTRACT. Reverse osmosis and nanofiltration by thin-film nanocomposite (TFN) membranes are energy-efficient processes for water purification. However, it is difficult to fabricate high-performance TFN membranes in controllable manner. In this work, the uniform and multilayered polyamide (PA)-graphene oxide (GO) TFN membranes were assembled by a simple and controllable strategy, named as multilayer deposition, which was performed by consecutively spin-coating GO, meta-phenylene diamine (MPD)/piperazine (PIP), and trimesoyl chloride (TMC) solutions on the substrates. The introduction of GO could reduce defects, resulting in formation of smooth and defect-free reverse osmosis/nanofiltration membranes with significantly increased NaCl and antibiotic rejection. For example, the TFN reverse osmosis membrane showed NaCl rejection of 99.1% and water permeance of 1.83 L m^{-2} h^{-1} bar^{-1}, accompanied by substantially enhanced antifouling property.

Keywords: Thin-film nanocomposite, Polyamide, Graphene oxide, Multilayer assembly, Water purification

1. Introduction

Reverse osmosis (RO) and nanofiltration (NF) membranes, featuring high energy efficiency and environmental friendliness compared to other competing separation technologies, have been widely employed to obtain fresh water through seawater desalination and wastewater reclamation [1-3]. The most common type of RO/NF membranes are polyamide (PA) thin-film composite (TFC) membranes that exhibit reasonable separation properties and stability. In the past decades, researchers have been attempting to overcome the permeability-selectivity upper bound by developing RO/NF membranes with higher permeance and higher rejection simultaneously [4,5]. One effective strategy is the inclusion of nanomaterials in PA to form thin-film nanocomposite (TFN) membranes. TFN membranes are fabricated by loading nanomaterials into amine and/or acyl chloride monomer solutions used for the interfacial polymerization (IP), which imparts enhanced separation performances and additional special functions (e.g., antifouling properties) [6-8].

Many kinds of nanomaterials with different dimensions including nanoparticles (e.g., silica [9,10] and metal-organic framework (MOF) nanoparticles [11-13]), nanowires/tubes (e.g., carbon nanotubes [14-16]), and nanosheets (e.g., carbon nitride [17] and covalent organic framework nanosheets [18]) have been used as nanofillers in TFN membranes to tailor transport channels for enhancing water permeation and obtaining high selectivity. For example, various ZnO nanostructures such as nanoflowers, nanorods, and spherical nanoparticles were embedded into PA layers for improving the desalination performance and antibacterial activity of TFN membrane. The spherical ZnO nanoparticles embedded TFN membrane displayed 19.0% and 28.4% higher water permeance than the membranes embedded with ZnO nanorods and nanoflowers, respectively, owing to higher surface area and smaller size of spherical nanoparticles [19]. To

provide more transport pathways for water molecules, defective ZIF-8 nanoparticles with additional inner porosity were used as nanofillers in TFN membranes, which endowed the membranes with a 52.0% increase in water permeance than the pristine TFC membrane while maintaining the NaCl rejection of 98.6% [20]. As one of the important derivatives of graphene, graphene oxide (GO) nanosheets possess many advantages including ultrathin thickness, excellent mechanical strength, low production cost, abundant functionality, and tunable physicochemical property [21-27]. The hydrophilic oxygen-containing functional groups and non-oxidized regions of GO can also accelerate the water transport through GO-based membranes. Due to these merits, GO nanosheets have been considered as promising alternative nanofillers to prepare high-performance TFN membranes [28-32].

Existing preparation approaches for PA-GO TFN membranes generally involve mixing GO nanosheets in aqueous/organic monomer solutions or depositing them on substrates [33-35]. Although the doping of nanomaterials in PA layers contributes to the improvement of water permeance, the easy aggregation of nanomaterials in polymeric matrixes poses a great challenge of potentially impaired rejection. Furthermore, the traditional IP reaction can be completed within ten seconds, thus making it difficult to control [36,37]. Multilayer assembly by step-by-step deposition is a controllable, versatile, and useful approach to precisely prepare uniform thin films on various substrates [38-42]. During multilayer assembly, each precursor solution is successively and repetitively coated on substrates to grow thin films of controllable thickness (e.g., by the number of coating cycles) [43,44]. Recently, the application of multilayer assembly strategy in TFN membrane usually focused on the post modification of PA layers through surface layer-by-layer coating, which could enhance the surface hydrophilicity and antifouling properties [3,39]. However, the compact surface coating layers may increase the diffusion resistance of water

molecules through TFN membranes. Considering the unique properties of GO, we envisage that whether GO can be embedded into PA layers during multilayer assembly of TFC membranes for preparing high-performance PA-GO TFN membranes in a more controllable and efficient manner.

In this work, we report a spin-coating multilayer assembly strategy for the preparation of PA-GO TFN membranes (Fig. 1). This strategy possesses advantages of easy operability, good controllability, and low solvent consumption. The deposited GO nanosheets provide stable and confined interface for PA polymerization, resulting in PA-GO TFN membranes with uniform, smooth, and defect-free rejection layers. These TFN membranes exhibit competitive desalination and antibiotic separation performance with substantially improved antifouling ability, paving a new direction for high performance TFN membranes.

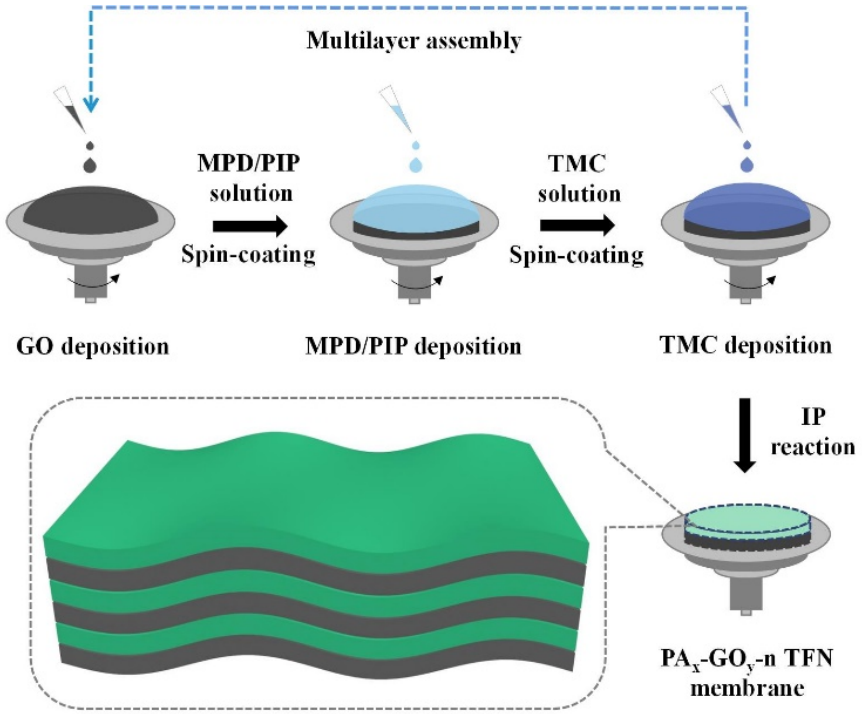

Fig. 1. Illustration of fabrication and structure of PA-GO TFN membranes by spin-coating multilayer assembly.

2. Experimental

2.1. Materials

Natural graphite flakes were purchased from XFnano Chemical Co., Ltd, China. Potassium permanganate ($KMnO_4$), sodium nitrate ($NaNO_3$), sulfuric acid (H_2SO_4, 98 wt%), hydrogen peroxide aqueous solution (H_2O_2, 30%), meta-phenylene diamine (MPD), piperazine (PIP), and trimesoyl chloride (TMC) were purchased from Kutai Chemical Reagent Co., China. The solvent of n-hexane was used without further purification. The polysulfone (PSF) ultrafiltration membrane with a molecular weight cutoff of 100 kDa was used as substrate.

2.2. Preparation of graphite oxide

The graphite oxide was prepared by a modified Hummers method [45]. Natural graphite flakes (2.0 g) and $NaNO_3$ (1.0 g) were gradually added into concentrated H_2SO_4 (46 mL) while in ice water bath. And then $KMnO_4$ (6.0 g) was slowly added into the above mixture under constant stirring and the mixture temperature was controlled below 20 ^oC. After reaction, the above suspension was further stirred at 35 ^oC for about 1 hour and pure deionized water of 96 mL was slowly added. The suspension temperature was heated to 98 ^oC for 40 min. Finally, the above suspension was treated by 30% H_2O_2 solution and washed by 5% HCl solution and deionized water. The obtained product was dried at 60 ^oC under vacuum for overnight to produce bulk graphite oxide.

2.3. Preparation of PA-GO RO membranes

A GO suspension was obtained by ultrasonic exfoliation of graphite oxide powder in water and then diluted to 0.1 mg/mL. PA-GO RO membranes were fabricated by the spin-coating multilayer assembly (Fig. 1). A 200 μL of the GO suspension was firstly dropped onto a polysulfone ultrafiltration membrane (PSF, molecular weight cutoff = 100 kDa) that was subjected

to rotation speed of 5000 rpm. For preparation of PA-GO RO membranes, a meta-phenylene diamine (MPD) aqueous solution (0.1 or 1.0 mg/mL) was spin-coated on the substrate by the same operation and then followed by a trimesoyl chloride (TMC) n-hexane solution (with a MPD/TMC concentration ratio of 10) to complete one deposition cycle. PA-GO RO membranes with different deposition cycles of 1, 3, 5, and 7 were prepared in the current study. Finally, the PA-GO RO membranes were dried at 60 ^{o}C for 5 minutes for better polymerization. The obtained PA-GO RO membranes are denoted as PA_x-GO_y-n membranes, where x, y, and n represent the MPD concentration, GO concentration, and deposition cycles, respectively. For comparison purpose, PA RO membranes were also prepared by same condition without GO suspension, and the corresponding membranes are denoted as PA_x-n.

2.4. Preparation of PA-GO NF membranes

PA-GO NF membranes were fabricated by the same spin-coating multilayer assembly as the PA-GO RO membranes. The GO suspension (0.1 mg/mL), piperazine (PIP) aqueous solution (0.1 mg/mL), and TMC n-hexane solution (0.1 mg/mL) were continuously spin-coated on the polysulfone substrate to complete one deposition cycle. PA-GO NF membranes with different deposition cycles of 1, 3, 5, and 7 were prepared in the current study. Finally, the PA-GO NF membranes were dried at 60 ^{o}C for 5 minutes for better polymerization. The obtained PA-GO NF membranes are denoted as PA_x-GO_y-n NF membranes, where x, y, and n represent the PIP concentration, GO concentration, and deposition cycles, respectively. For comparison purpose, PA NF membranes without GO were also prepared by same condition.

2.5. Characterizations

The morphologies of the prepared PA-GO TFN membranes were observed by a field-emission scanning electron microscope (SEM, Ultra-55, Zeiss Co.) at an accelerating voltage of 5

kV. The samples were coated with thin gold layers to reduce the charging effect. The surface structures of the PA-GO membranes were characterized by employing an atomic force microscope (AFM, Bioscope Catalyst Nanoscope-V, Bruker, USA). The values of root mean square roughness (Rq) and arithmetic average roughness (Ra) were calculated by NanoScope Analysis software. The chemical structures of the samples were studied by using Fourier transform infrared spectrometer (FTIR, IRTracer-100, Shimadzu CO.). X-ray photoelectron spectroscopy (XPS) experiments were conducted by using an RBD upgraded PHI-5000C ESCA system (PerkinElmer). The hydrophilic properties were investigated by using a contact angle meter (OCA20/data-physics, Germany). The water contact angle was measured for at least three samples to obtain the average value. Surface zeta potentials of membranes were evaluated using streaming potential analyzer (SurPASS, Anton Paar, Austria) with 1mmol/L KCl aqueous solution as the background electrolyte. The solution pH was controlled by using HCl and NaOH solutions to measure the zeta potential values at pH of 4–10.

2.6. Desalination performance test

The desalination performance of the prepared PA-GO RO membranes was investigated by a cross-flow filtration cell with an effective permeation area of 7.0 cm^2. The desalination experiment was conducted using a 2000 mg/L NaCl solution as the feed with an applied pressure of 10 bar at room temperature. The concentration of NaCl solution was measured by a conductivity meter. The water permeance (P, L m^{-2} h^{-1} bar^{-1}) and NaCl rejection (R) of the membranes were calculated according to the following equations (1) and (2), respectively:

$$P = \frac{V}{A \times t \times \Delta p} \quad (1)$$

$$R = \left(1 - \frac{C_p}{C_f}\right) \times 100\% \quad (2)$$

Where V (L) is the permeated water volume, A (m^2) is the effective membrane area, t (h) is the permeated time, and Δp is the transmembrane pressure. The parameters C_f and C_p are the salt concentrations in the feed and permeate solutions, respectively. The reported permeance and rejection results for each membrane were the average of at least three membrane samples.

2.7. Nanofiltration performance test

The nanofiltration performance of the prepared PA-GO NF membranes was investigated by a cross-flow filtration cell with an effective membrane area of 7.0 cm^2. The nanofiltration test was conducted employing chlortetracycline aqueous solution (100 mg/L) as the feed with an applied pressure of 4 bar at room temperature. The concentration of chlortetracycline solution was measured by UV characterization.

2.8. Membrane fouling test

Membrane fouling and cleaning properties were investigated by using sodium alginate (SA) as model organic foulants. The prepared PA-GO RO membranes were first equilibrated with the foulant-free background electrolyte solution (1 mM $CaCl_2$ + 47 mM NaCl) under pressure at room temperature until water permeance became stable. For conducting membrane fouling test, a SA stock solution was then added into the feed tank to obtain a final feed foulant concentration of 200 mg/L. After running for 360 min, the feed solution was replaced with DI water to flush the membranes for removing the foulant. The pure water permeances of the membranes were then measured to evaluate the fouling reversibility of membranes.

3. Results and Discussion

3.1. Characterizations of PA-GO TFN membranes

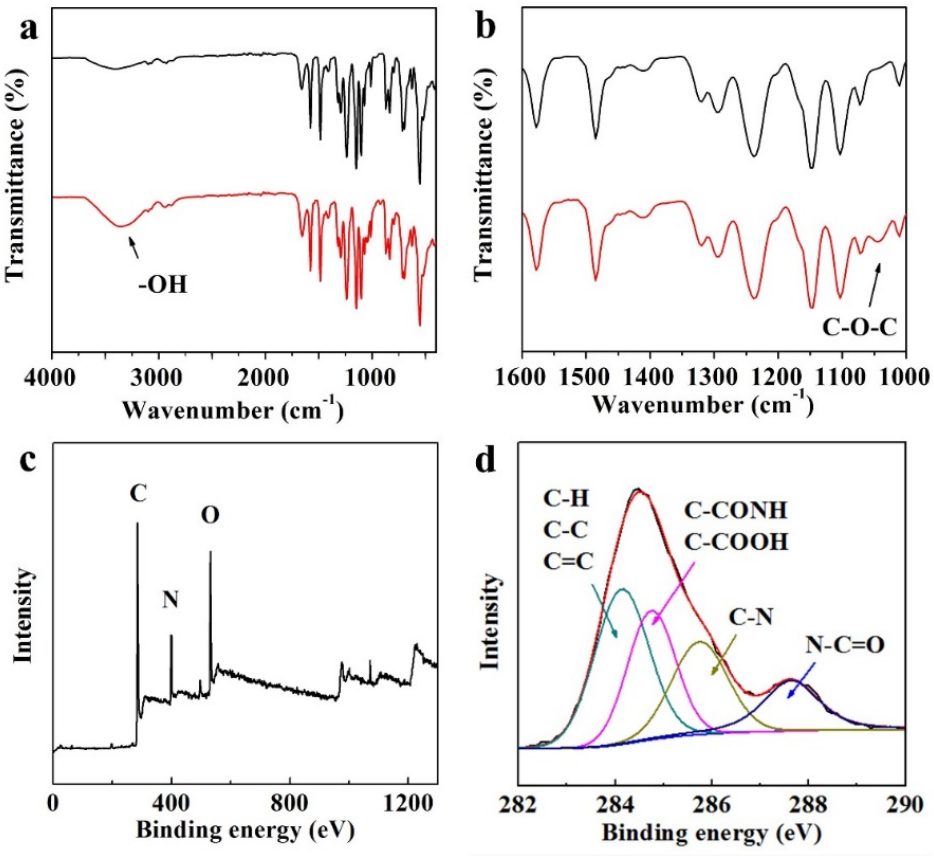

Fig. 2. (a and b) FTIR spectra of the PA_1-5 (black) and PA_1-$GO_{0.1}$-5 (red) RO membranes. (c) XPS spectrum and (d) high-resolution C 1s XPS spectra of the PA_1-$GO_{0.1}$-5 RO membrane.

For fabrication of the PA-GO RO membranes, the GO suspension (0, 0.1, or 1.0 mg/mL), MPD aqueous solution (0.1 or 1.0 mg/mL), and TMC n-hexane solution (with MPD/TMC ratio of 10) were consecutively spin-coated on the PSF substrates (Fig. 1). In the current study, the solvent consumption was as low as 200 μL for each coating cycle, which was much lower relative to the conventional IP process [29,46]. Fig. 2a,b presents the FTIR spectra of the PA_1-5 and PA_1-$GO_{0.1}$-5 RO membranes. Both membranes showed characteristic peaks at 1659, 1578, and 1485 cm^{-1}, which can be assigned to the stretching vibration of C=O, N-H, and C-N, respectively, proving the successful preparation of polyamide selective layer. PA_1-$GO_{0.1}$-5 had a much more intense peak at 3364 cm^{-1} compared to PA_1-5, resulting from the embedding of GO nanosheets with abundant

–OH groups. Concomitantly, a new characteristic peak at 1045 cm^{-1} emerged in the spectrum of PA_1-$GO_{0.1}$-5, which is assigned to the epoxy groups of GO. These results verified the successful incorporation of GO nanosheets into the TFN membranes. The XPS spectra were employed to identify the PA polymerization. Compared with the PSF substrate (Fig. S1), a new peak of N 1s appeared at binding energy of 399.6 eV in the spectrum of the PA_1-$GO_{0.1}$-5 membrane (Fig. 2c), ascribing to the formation of PA layer. Since the membrane surface was completely covered by the PA-GO layer, the S 2p peak of the PSF substrate almost disappeared after multilayer assembly. The high-resolution C 1s spectra with four fitting peaks at 284.2 eV (C-H, C-C, and C=C), 284.8 eV (C-CONH and C-COOH), 285.8 eV (C-N), and 287.7 eV (N-C=O) confirmed the successful PA polymerization based on Schotten-Baumann reaction between acyl chloride and amino (Fig. 2d).

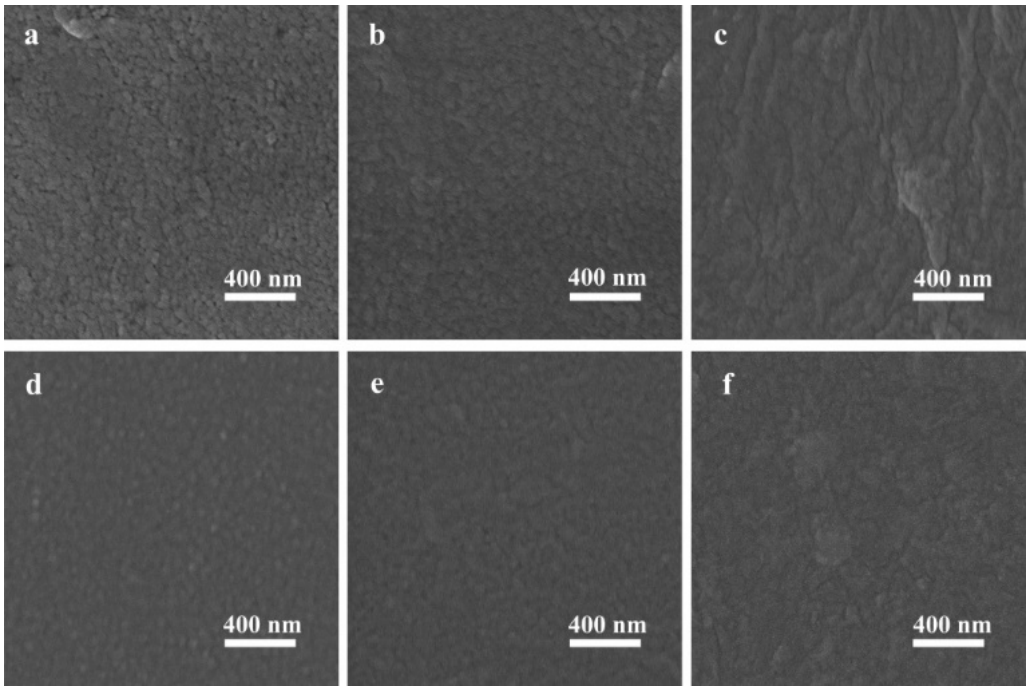

Fig. 3. SEM images of (a) $PA_{0.1}$-5, (b) $PA_{0.1}$-$GO_{0.1}$-5, (c) $PA_{0.1}$-GO_1-5, (d) PA_1-5, (e) PA_1-$GO_{0.1}$-5 and (f) PA_1-GO_1-5 RO membranes.

Fig. 3 shows the SEM images of the PA and PA-GO RO membranes with same spin-coating deposition cycles of 5 but different MPD and GO concentrations. The PA membrane with low MPD concentration ($PA_{0.1}$-5) appeared discontinuous and defective (Fig. 3a), possibly due to the penetration of the MPD aqueous solution into porous PSF substrate [43,47]. In contrast, the GO containing RO membrane $PA_{0.1}$-$GO_{0.1}$-5 showed a defect-free and granular structure (Fig. 3b), revealing the critical role of GO deposition in the formation of a continuous PA layer. GO nanosheets provide stable reaction interface, prevent monomer solution penetration into substrate, and improve MPD storage for better interfacial polymerization. The resulted granular structure may be originated from the higher affinity of MPD molecules to the oxygen-containing groups on GO nanosheets, thereby leading to the preferential polymerization of PA on these regions. With the increase of GO concentration to 1.0 mg/mL, the $PA_{0.1}$-GO_1-5 membrane displayed some wrinkles (Fig. 3c), which are often observed in pure GO membranes [48,49]. As expected, the increase of MPD concentration could also promote the formation of continuous PA membranes (see PA_1-5 in Fig. 3d). As GO concentration increased to 1.0 mg/mL, wrinkles also appeared for the membrane PA_1-GO_1-5 (Fig. 3f), though they were less obvious compared with $PA_{0.1}$-GO_1-5. Additional PA-GO membranes PA_1-$GO_{0.1}$-n (with MPD concentration fixed at 1.0 mg/mL, GO concentration fixed at 0.1 mg/mL, and over different deposition cycles) are presented in Fig. S2 in the supporting information. Clearly, as the number of deposition cycle increased, the prepared PA-GO RO membranes became more continuous with a denser surface. We also conducted the cross-sectional SEM characterization of the PA_1-$GO_{0.1}$ RO membranes. As shown in Fig. S3, when depositing 3 cycles, the PA_1-$GO_{0.1}$-3 RO membrane showed an ultrathin thickness at about 80 nm. By increasing deposition cycles, the thickness of PA_1-$GO_{0.1}$-7 membrane increased to 160 nm.

Although greater thickness usually resulted in better continuity, smaller thickness brought higher water permeance.

Unlike PA membranes prepared by conventional IP that possess rough surface with leaf-like features, the multilayer-deposited PA membrane was much smoother due to the multistep micro-polymerization from the step-by-step coating (Fig. 3 and 4). AFM characterization of the PA_1-5 membrane and PA_1-$GO_{0.1}$-1, PA_1-$GO_{0.1}$-5 and PA_1-$GO_{0.1}$-7 membranes shows that these membranes had Rq < 5.0 nm and Ra < 4.0 nm, which are much lower than those of PA membranes prepared by conventional IP [50-52]. Compared to the PA_1-5 membrane (Rq = 4.60 nm and Ra = 3.65 nm), the PA_1-$GO_{0.1}$-5 membrane with identical number of deposition cycle had slightly reduced surface roughness (Rq = 3.39 nm and Ra = 2.69 nm). This may be interpreted by that the GO nanosheets offer more stable and confined interface for polymerization. In addition, as the deposition cycle increased from 1 to 7, the PA-GO membranes also became smoother, with Rq decreased from 3.71 nm to 3.02 nm and Ra decreased from 2.96 nm to 2.46 nm. The inclusion of GO nanosheets (Fig. S4) or increasing the deposition cycle (Fig. S5) were also effective in reducing the water contact angle due to the oxygen-containing groups of GO nanosheets, which is beneficial for enhanced separation performance [53]. The surface charges of the PA and PA-GO membranes were measured by the zeta potential analysis. As shown in Fig. S6, both PA and PA-GO membrane surfaces possessed negative charges in the pH range of 4–10, due to existence of the carboxyl groups arising from the hydrolysis of residual acyl chloride groups. In contrast with PA membrane, the PA-GO membrane had more negative charges, which should result from the introduction of GO containing numerous negatively charged functional groups [33].

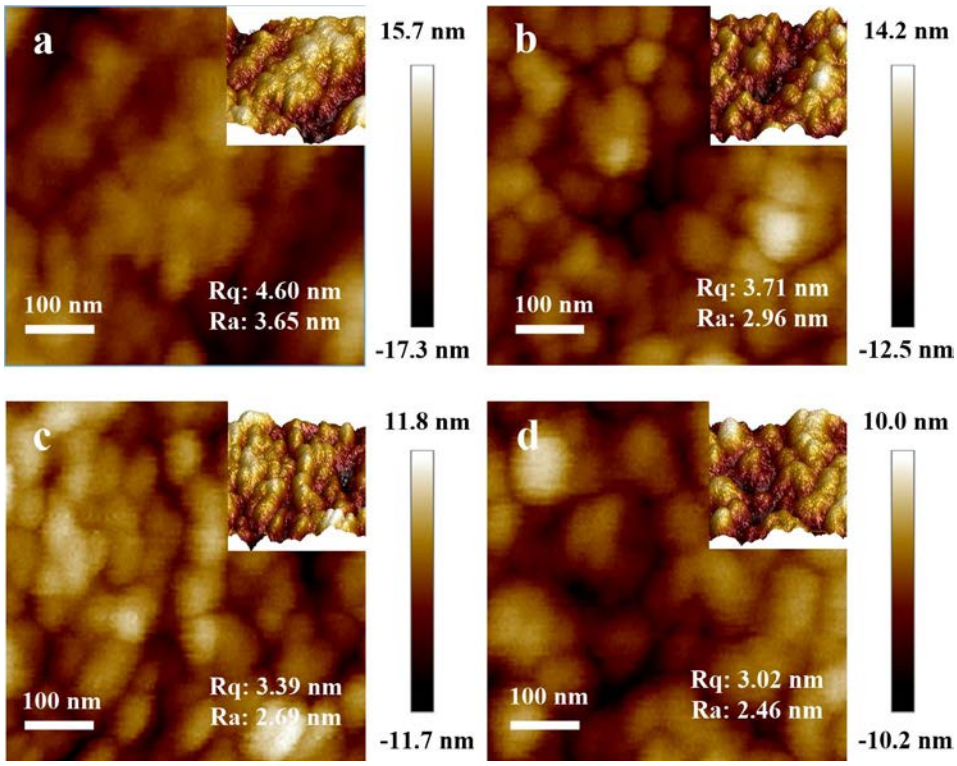

Fig. 4. AFM images of the PA ((a) PA_1-5) and PA-GO RO membranes ((b) PA_1-$GO_{0.1}$-1, (c) PA_1-$GO_{0.1}$-5, and (d) PA_1-$GO_{0.1}$-7). The insets were corresponding 3D AFM images of membranes.

3.2. Desalination performance

Membrane separation performance was evaluated by cross-flow filtration using a 2000 mg/L NaCl solution (Fig. 5). For membranes prepared at any given MPD and GO concentrations, increasing deposition cycles sharply decreased the water permeance and increased the NaCl rejection, which can be attributed to the more continuous and thicker selective layers [43]. For the $PA_{0.1}$-n series, the rejection remained relatively low (84.8%) even after deposition for 7 cycles. The addition of GO nanosheets was able to substantially improve the membrane rejection, with $PA_{0.1}$-$GO_{0.1}$-7 and $PA_{0.1}$-GO_1-7 showing NaCl rejections of 94.1% and 92.6%, respectively. The crumpled GO nanosheets of the PA-GO RO membranes with high GO loading may result in

unselective pathways for ion transports, which explains the slightly lower rejection of $PA_{0.1}$-GO_1-7 compared to $PA_{0.1}$-$GO_{0.1}$-7.

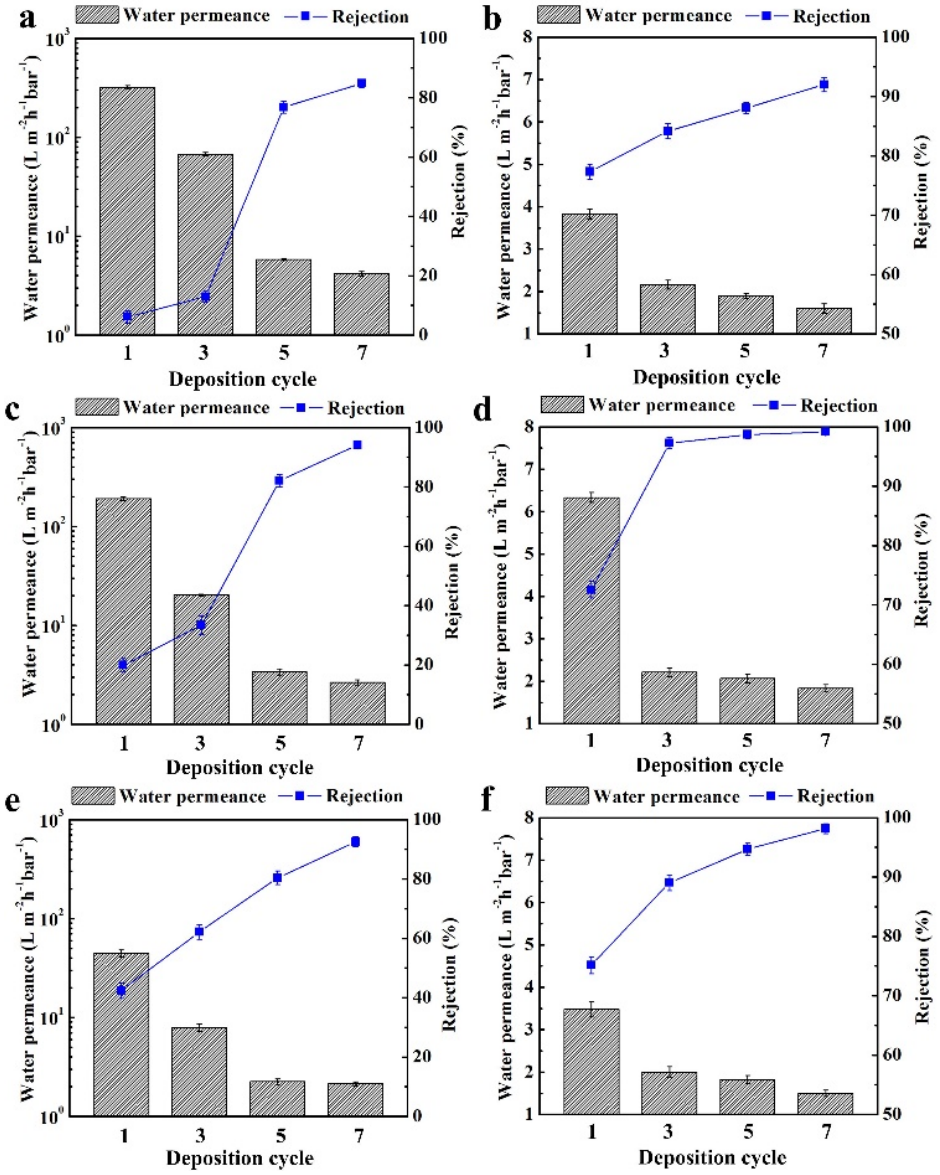

Fig. 5. Desalination performances of (a) $PA_{0.1}$-n, (b) PA_1-n, (c) $PA_{0.1}$-$GO_{0.1}$-n, (d) PA_1-$GO_{0.1}$-n, (e) $PA_{0.1}$-GO_1-n, and (f) PA_1-GO_1-n RO membranes with various deposition cycles of n. The error bar was standard deviation calculated from three membrane samples at least.

All membranes formed with 1.0 mg/mL MPD, including PA_1-n (Fig. 5b), PA_1-$GO_{0.1}$-n (Fig. 5d), and PA_1-GO_1-n (Fig. 5f), exhibited higher rejection and lower permeance compared to their respective counterparts formed with 0.1 mg/mL MPD. In particular, the PA_1-$GO_{0.1}$-n series appeared most promising in terms of rejection performance. Even deposition for only 3 cycles, the PA_1-$GO_{0.1}$-3 RO membrane showed a high rejection of 97.3% and permeance of 2.21 L m^{-2} h^{-1} bar^{-1}. By increasing deposition cycles, the PA_1-$GO_{0.1}$-7 membrane showed an impressive rejection of 99.1% together with a permeance of 1.83 L m^{-2} h^{-1} bar^{-1}. These separation properties are highly competitive against existing commercial RO membranes (Fig. S7) and other TFN membranes in the reported literatures (Table S1) by exceeding the permeability-selectivity trade-off [54]. The effect of feed concentration on desalination performance of the PA-GO membranes was also assessed. Although the higher osmotic pressure and more serious concentration polarization at high feed concentration caused a reduction of permeance, the PA-GO membranes exhibited stable and even larger rejection (Fig. S8). We conducted the desalination test of PA_1-$GO_{0.1}$-7 RO membrane at various pH values of 4, 7, and 10. The results showed that the water permeance of membrane was independent of feed pH while rejection rate increased from 98.4 to 99.3% with increasing feed pH from 4 to 10. This may be attributed to the stronger electrostatic repulsion interactions at higher pH, as arising from increasingly negative charges on the membrane surfaces [55].

3.3. Antifouling property

The fouling behavior of the PA_1-7 and PA_1-$GO_{0.1}$-7 RO membranes were evaluated using SA as model foulant. As shown in Fig. 6a, the PA_1-$GO_{0.1}$-7 membrane presented lower water permeance reduction ratio (17.8%) in contrast with that (26.9%) of the PA_1-7 membrane, despite that PA_1-$GO_{0.1}$-7 had a higher initial water permeance (1.65 L m^{-2} h^{-1} bar^{-1} for PA_1-$GO_{0.1}$-7 vs. 1.43 L m^{-2} h^{-1} bar^{-1} for PA_1-7). Fouling reversibility property was also investigated by flushing the

fouled membranes with DI water for 60 min. The PA-GO membrane displayed higher water permeance recovery ratio than that of the PA membrane. These results strongly suggest that PA-GO membranes possessed better antifouling performance, which can be attributed to more hydrophilic and smoother membrane surfaces due to introduction of GO [34]. Membrane long-term stability is one of the critical concerns when developing PA membrane for practical application. We investigated the stability of the PA-GO RO membrane by running for 48 hours. The membrane showed stable water permeance and salt rejection during the entire filtration time (Fig. S9), proving the excellent stability of the prepared PA-GO membrane.

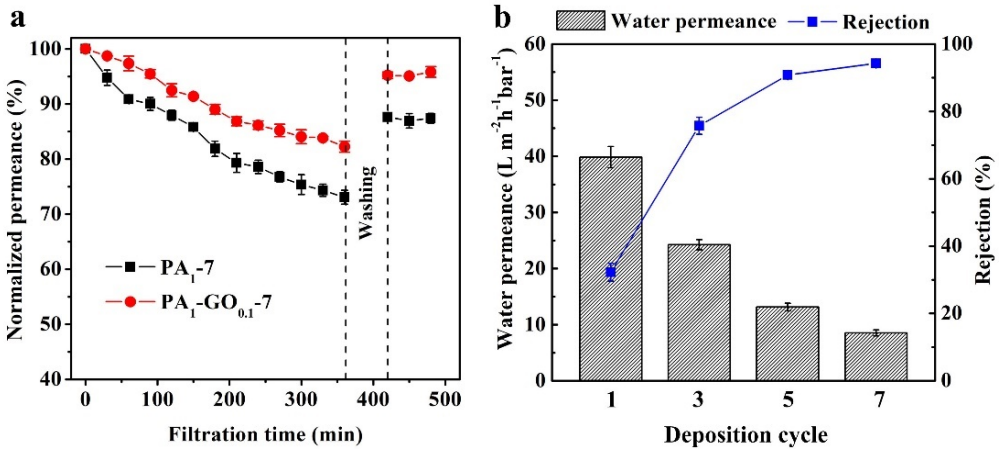

Fig. 6. (a) The fouling and fouling reversibility for the PA_1-7 and PA_1-$GO_{0.1}$-7 RO membranes using sodium alginate (SA, 200 mg/L) as model foulant. The initial water permeances of PA_1-7 and PA_1-$GO_{0.1}$-7 membranes were 1.43 and 1.65 L m^{-2} h^{-1} bar^{-1}, respectively. (b) Water permeance and chlortetracycline rejection of $PA_{0.1}$-$GO_{0.1}$-n NF membranes with various deposition cycles of n.

3.4. Applicability of multilayer assembly

In order to demonstrate the general applicability of spin-coating multilayer assembly strategy and show the nanofiltration application of the prepared membranes, the multilayered PA-GO NF membranes with various deposition cycles were prepared by consecutively spin-coating GO, PIP,

and TMC solutions on the polysulfone substrates. As shown in Fig. S10, the $PA_{0.1}$-$GO_{0.1}$-7 NF membrane showed smooth surfaces along with some wrinkles from GO nanosheets, which were not appeared in $PA_{0.1}$-7 membrane. We also evaluated the antibiotic separation performances of PA-GO NF membranes employing chlortetracycline aqueous solution at 4 bar. For PA-GO NF membranes, increasing deposition cycles would decrease the water permeance and significantly increase the chlortetracycline rejection (Fig. 6b). After coating for 5 cycles, the $PA_{0.1}$-$GO_{0.1}$-5 NF membrane showed large water permeance of 13.1 L m^{-2} h^{-1} bar^{-1} and chlortetracycline rejection of 90.8%. As coating cycle increased to 7, the $PA_{0.1}$-$GO_{0.1}$-7 NF membrane displayed a higher rejection of 94.3% along with a permeance of 8.54 L m^{-2} h^{-1} bar^{-1}. For the pure $PA_{0.1}$-7 NF membrane without GO, water permeance reduced to 7.49 L m^{-2} h^{-1} bar^{-1} with a relatively low rejection of 90.2%. These results demonstrate that the multilayer assembly strategy is available for obtaining nanofiltration membranes with good antibiotic separation performance.

The multilayer assembly also shows good potential in many other aspects. For example, this approach could be potentially extended to other TFN membrane chemistries, such as interfacial polymerization by other amines and TMC [14,53], to target a wider range of contaminants and separation processes. Future studies may also explore additional applications beyond simple desalination and antibiotic separation, such as the removal of toxic organic micropollutants for water reuse. In addition, membrane performance may be further improved by tailoring the physicochemical properties of substrates, adjusting synthesis parameters, and replacing GO nanosheets with porous nanomaterials [56,57]. In general, the multilayer assembly reported here can be an excellent candidate to prepare high-performance TFN membrane for water treatment.

3.5. Mechanism analysis

In comparison with the PA TFC membranes, the PA-GO TFN membranes exhibited greater rejection, higher permeance, and enhanced antifouling performance. The greater rejection may be attributed to the formation of denser and more uniform selective layers. During the preparation of the PA TFC membranes, the small amount of the loaded MPD/PIP and TMC molecules and the infiltration of these monomer solutions into the porous substrates make it difficult to form continuous and uniform PA layers (Fig. 7a). For the PA-GO TFN membranes, the incorporated GO nanosheets may serve three functions to promote the formation of defect-free membranes (Fig. 7b): (1) the GO nanosheets can increase the storage of MPD/PIP molecules due to their large number of oxygen-containing groups, thereby promoting the PA polymerization; (2) the deposited GO layers can provide stable interfaces and then facilitate the formation of more uniform PA-GO layers; and (3) the small pore size of the GO layers slow the diffusion of MPD/PIP molecules and reduce the intensity of Schotten-Baumann reaction for better polymerization [58,59].

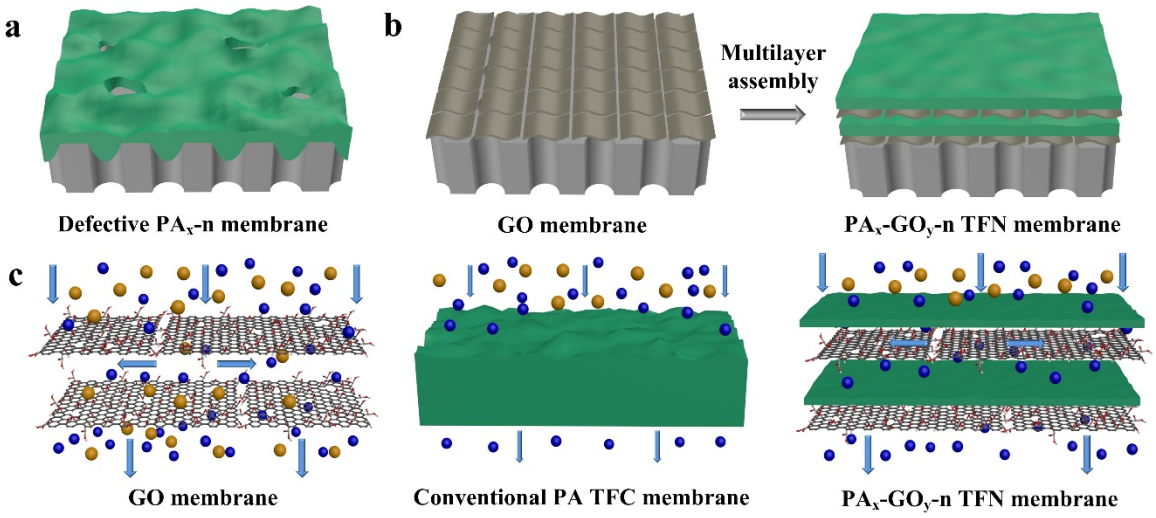

Fig. 7. Schematics of multilayer assembly of (a) defective PA_x-n and (b) defect-free PA_x-GO_y-n TFN membranes, and (c) molecular transport through GO, conventional PA TFC, and PA_x-GO_y-n TFN membranes.

GO nanosheets also play an important role in the permeance of the PA-GO TFN membranes (Fig. 7c). For pure GO membranes, all interlayer channels, inner pores, and inter-edge spaces can be served as pathways for molecular transports [27,60]. Typically, GO possesses highly oxidized and non-oxidized regions in molecular skeletons. The oxygen-containing groups can help adjacent GO nanosheets to form interlayer transport channels and promote water molecules to quickly pass through GO membranes in hydrated state. Moreover, the existence of non-oxidized regions in GO can construct rapid capillary networks, which facilitate correlated water transport through the membranes as nearly frictionless flow. All these facts result in the ultrahigh water permeance of GO membranes. For the conventional PA TFC membranes, the trimesoyl chloride and amine interfacial reaction produces highly crosslinked and dense polyamide network, rejecting the passage of salt ions or antibiotics while showing relatively low water permeation. Compared with the conventional PA TFC membranes governed by solution-diffusion mechanism, the insertion of GO nanosheets endows the PA-GO TFN membranes with interlayer channels and capillary networks for rapid water transport [28,29]. The multilayered structure of PA-GO TFN membranes may also be beneficial to the enhancement in water permeance. Moreover, because of the more hydrophilic and smoother surfaces from the introduction of GO in PA layers, the antifouling property of PA-GO TFN membranes is enhanced.

4. Conclusion

In this study, we report the simple multilayer assembly strategy for preparation of PA-GO reverse osmosis/nanofiltration membranes. Benefiting from the stepwise polymerization and nanomaterial incorporation, the formation processes and membrane structures can be controlled more effectively. The insertion of GO nanosheets by multilayer assembly improves the monomer adsorption and offers stable interface, promoting the formation of uniform and defect-free TFN

membranes with increased NaCl and antibiotic rejection. The prepared PA-GO RO membrane displayed the impressive NaCl rejection of 99.1% and water permeance of 1.83 L m^{-2} h^{-1} bar^{-1}, accoupled with enhanced antifouling property. Overall, the multilayer assembly reported here provides a promising alternative route to fabricate high-performance TFN membrane for water purification.

Supporting information.

Characterizations (SEM, XPS, and water contact angles) and desalination performance of PA TFC and PA-GO TFN membranes.

Acknowledgements

This work was financially supported by the Guangdong Basic and Applied Basic Research Foundation (Grant No. 2020B1515120036) and the Hong Kong Scholars Program (Grant No. XJ2019046). The work is also partially supported by a grant from the Research Grants Council of the Hong Kong Special Administrative Region, China (GRF HKU 17204220).

References

[1] Z. Tan, S. Chen, X. Peng, L. Zhang, C. Gao, Polyamide membranes with nanoscale turing structures for water purification, Science 360 (2018) 518-521.

[2] Z. Yang, P. Sun, X. Li, B. Gan, L. Wang, X. Song, H. Park, C. Tang, A critical review on thin-film nanocomposite membranes with interlayered structure: mechanisms, recent developments, and environmental applications, Environ. Sci. Technol. 54 (2020) 15563-15583.

[3] N.A. Ahmad, P.S. Goh, K.C. Wong, A.K. Zulhairun, A.F. Ismail, Enhancing desalination performance of thin film composite membrane through layer by layer assembly of oppositely charged titania nanosheet, Desalination 476 (2020) 114167.

[4] R. Zhang, J. Tian, S. Gao, B. Van der Bruggen, How to coordinate the trade-off between water permeability and salt rejection in nanofiltration, J. Mater. Chem. A 8 (2020) 8831-8847.

[5] H.B. Park, J. Kamcev, L.M. Robeson, M. Elimelech, B.D. Freeman, Maximizing the right stuff: The trade-off between membrane permeability and selectivity, Science 356 (2017) eaab0530.

[6] H. Saleem, S.J. Zaidi, Nanoparticles in reverse osmosis membranes for desalination: A state of the art review, Desalination 475 (2020) 114171.

[7] M. Ma, C. Zhang, C. Zhu, S. Huang, J. Yang, Z. Xu, Nanocomposite membranes embedded with functionalized MoS_2 nanosheets for enhanced interfacial compatibility and nanofiltration performance, J. Membr. Sci. 591 (2019) 117316.

[8] D.L. Zhao, S. Japip, Y. Zhang, M. Weber, C. Maletzko, T.S. Chung, Emerging thin-film nanocomposite (TFN) membranes for reverse osmosis: A review, Water Res. 173 (2020) 115557.

[9] M. Bao, G. Zhu, L. Wang, M. Wang, C. Gao, Preparation of monodispersed spherical mesoporous nanosilica-polyamide thin film composite reverse osmosis membranes via interfacial polymerization, Desalination 309 (2013) 261-266.

[10] H. Shen, S. Wang, H. Xu, Y. Zhou, C. Gao, Preparation of polyamide thin film nanocomposite membranes containing silica nanoparticles via an in-situ polymerization of $SiCl_4$ in organic solution, J. Membr. Sci. 565 (2018) 145-156.

[11] J. Zhu, L. Qin, A. Uliana, J. Hou, J. Wang, Y. Zhang, X. Li, S. Yuan, J. Li, M. Tian, J. Lin, B. Van der Bruggen, Elevated performance of thin film nanocomposite membranes enabled by modified hydrophilic MOFs for nanofiltration, ACS Appl. Mater. Interfaces 9 (2017) 1975-1986.

[12] Z. Wang, Z. Wang, S. Lin, H. Jin, S. Gao, Y. Zhu, J. Jin, Nanoparticle-templated nanofiltration membranes for ultrahigh performance desalination, Nat. Commun. 9 (2018) 2004.

[13] Y. Zhao, Y. Liu, X. Wang, X. Huang, Y.F. Xie, Impacts of metal-organic frameworks on structure and performance of polyamide thin-film nanocomposite membranes, ACS Appl. Mater. Interfaces 11 (2019) 13724-13734.

[14] F.Y. Zhao, Y.L. Ji, X.D. Weng, Y.F. Mi, C.C. Ye, Q.F. An, C.J. Gao, High-flux positively charged nanocomposite nanofiltration membranes filled with poly(dopamine) modified multiwall carbon nanotubes, ACS Appl. Mater. Interfaces 8 (2016) 6693-6700.

[15] H. Wu, H. Sun, W. Hong, L. Mao, Y. Liu, Improvement of polyamide thin film nanocomposite membrane assisted by tannic acid-FeIII functionalized multiwall carbon nanotubes, ACS Appl. Mater. Interfaces 9 (2017) 32255-32263.

[16] R. Cruz-Silva, Y. Takizawa, A. Nakaruk, M. Katouda, A. Yamanaka, J. Ortiz-Medina, A. Morelos-Gomez, S. Tejima, M. Obata, K. Takeuchi, T. Noguchi, T. Hayashi, M. Terrones, M. Endo, New insights in the natural organic matter fouling mechanism of polyamide and nanocomposite multiwalled carbon nanotubes-polyamide membranes, Environ. Sci. Technol. 53 (2019) 6255-6263.

[17] X. Gao, Y. Li, X. Yang, Y. Shang, Y. Wang, B. Gao, Z. Wang, Highly permeable and antifouling reverse osmosis membranes with acidified graphitic carbon nitride nanosheets as nanofillers, J. Mater. Chem. A 5 (2017) 19875-19883.

[18] L. Xu, B. Shan, C. Gao, J. Xu, Multifunctional thin-film nanocomposite membranes comprising covalent organic nanosheets with high crystallinity for efficient reverse osmosis desalination, J. Membr. Sci. 593 (2020) 117398.

[19] R. Rajakumaran, M. Kumar, R. Chetty, Morphological effect of ZnO nanostructures on desalination performance and antibacterial activity of thin-film nanocomposite (TFN) membrane, Desalination 495 (2020) 114673.

[20] Q. Zhao, D.L. Zhao, T.S. Chung, Thin-film nanocomposite membranes incorporated with defective ZIF-8 nanoparticles for brackish water and seawater desalination, J. Membr. Sci. 625 (2021) 119158.

[21] V. Vatanpour, A. Sanadgol, Surface modification of reverse osmosis membranes by grafting of polyamidoamine dendrimer containing graphene oxide nanosheets for desalination improvement, Desalination 491 (2020) 114442.

[22] L. Chen, G. Shi, J. Shen, B. Peng, B. Zhang, Y. Wang, F. Bian, J. Wang, D. Li, Z. Qian, G. Xu, G. Liu, J. Zeng, L. Zhang, Y. Yang, G. Zhou, M. Wu, W. Jin, J. Li, H. Fang, Ion sieving in graphene oxide membranes via cationic control of interlayer spacing, Nature 550 (2017) 380-383.

[23] W. Li, W. Wu, Z. Li, Controlling interlayer spacing of graphene oxide membranes by external pressure regulation, ACS Nano 12 (2018) 9309-9317.

[24] W. Wu, J. Su, M. Jia, W. Zhong, Z. Li, W. Li, Ultrastable sandwich graphene oxide hollow fiber membranes with confined interlayer spacing, J. Mater. Chem. A 7 (2019) 13007-13011.

[25] L. Wang, N. Wang, J. Li, J. Li, W. Bian, S. Ji, Layer-by-layer self-assembly of polycation/GO nanofiltration membrane with enhanced stability and fouling resistance, Sep. Purif. Technol. 160 (2016) 123-131.

[26] J. Su, M. Jia, W. Wu, Z. Li, W. Li, Chemical vapor crosslinking of graphene oxide membranes for controlling nanochannels, Environ. Sci.: Nano 7 (2020) 2924-2929.

[27] P. Su, F. Wang, Z. Li, C.Y. Tang, W. Li, Graphene oxide membranes: Controlling their transport pathways, J. Mater. Chem. A 8 (2020) 15319-15340.

[28] S. Bano, A. Mahmood, S. Kim, K. Lee, Graphene oxide modified polyamide nanofiltration membrane with improved flux and antifouling properties, J. Mater. Chem. A 3 (2015) 2065-2071.

[29] J. Yin, G. Zhu, B. Deng, Graphene oxide (GO) enhanced polyamide (PA) thin-film nanocomposite (TFN) membrane for water purification, Desalination 379 (2016) 93-101.

[30] P. Wen, Y. Chen, X. Hu, B. Cheng, D. Liu, Y. Zhang, S. Nair, Polyamide thin film composite nanofiltration membrane modified with acyl chlorided graphene oxide, J. Membr. Sci. 535 (2017)

208-220.

[31] C. Cheng, P. Li, K. Shen, T. Zhang, X. Cao, B. Wang, X. Wang, B.S. Hsiao, Integrated polyamide thin-film nanofibrous composite membrane regulated by functionalized interlayer for efficient water/isopropanol separation, J. Membr. Sci. 553 (2018) 70-81.

[32] F. Yu, H. Shi, J. Shi, K. Teng, Z. Xu, X. Qian, High-performance forward osmosis membrane with ultra-fast water transport channel and ultra-thin polyamide layer, J. Membr. Sci. 616 (2020) 118611.

[33] H. Chae, J. Lee, C. Lee, I. Kim, P. Park, Graphene oxide-embedded thin-film composite reverse osmosis membrane with high flux, anti-biofouling, and chlorine resistance, J. Membr. Sci. 483 (2015) 128-135.

[34] J. Shi, W. Wu, Y. Xia, Z. Li, W. Li, Confined interfacial polymerization of polyamide-graphene oxide composite membranes for water desalination, Desalination 441 (2018) 77-86.

[35] N. Song, Y. Sun, X. Xie, D. Wang, F. Shao, L. Yu, L. Dong, Doping MIL-101(Cr)@GO in polyamide nanocomposite membranes with improved water flux, Desalination 492 (2020) 114601.

[36] V. Freger, Nanoscale heterogeneity of polyamide membranes formed by interfacial polymerization, Langmuir 19 (2003) 4791-4797.

[37] P.M. Johnson, J. Yoon, J.Y. Kelly, J.A. Howarter, C.M. Stafford, Molecular layer-by-layer deposition of highly crosslinked polyamide films, J. Polym. Sci., Part B: Polym. Phys. 50 (2012) 168-173.

[38] W. Ma, A. Soroush, T. Van Anh Luong, G. Brennan, M.S. Rahaman, B. Asadishad, N. Tufenkji, Spray- and spin-assisted layer-by-layer assembly of copper nanoparticles on thin-film composite reverse osmosis membrane for biofouling mitigation, Water Res. 99 (2016) 188-199.

[39] F. Shao, C. Xu, W. Ji, H. Dong, Q. Sun, L. Yu, L. Dong, Layer-by-layer self-assembly TiO_2

and graphene oxide on polyamide reverse osmosis membranes with improved membrane durability, Desalination 423 (2017) 21-29.

[40] Q. Li, G. Q. Chen, L. Liu, S. E. Kentish, Spray assisted layer-by-layer assembled one-bilayer polyelectrolyte reverse osmosis membranes, J. Membr. Sci. 564 (2018) 501-507.

[41] M. Abbaszadeh, D. Krizak, S. Kundu, Layer-by-layer assembly of graphene oxide nanoplatelets embedded desalination membranes with improved chlorine resistance, Desalination 470 (2019) 114116.

[42] W. D. Mulhearn, V. P. Oleshko, C. M. Stafford, Thickness-dependent permeance of molecular layer-by-layer polyamide membranes, J. Membr. Sci. 618 (2021) 118637.

[43] J.E. Gu, S. Lee, C.M. Stafford, J.S. Lee, W. Choi, B.Y. Kim, K.Y. Baek, E.P. Chan, J.Y. Chung, J. Bang, J.H. Lee, Molecular layer-by-layer assembled thin-film composite membranes for water desalination, Adv. Mater. 25 (2013) 4778-4782.

[44] F. Fadhillah, S.M.J. Zaidi, Z. Khan, M.M. Khaled, F. Rahman, P.T. Hammond, Development of polyelectrolyte multilayer thin film composite membrane for water desalination application, Desalination 318 (2013) 19-24.

[45] D.C. Marcano, D.V. Kosynkin, J.M. Berlin, A. Sinitskii, Z. Sun, A. Slesarev, L.B. Alemany, W. Lu, J.M. Tour, Improved synthesis of graphene oxide, ACS Nano 4 (2010) 4806-4814.

[46] J.R. Ray, S. Tadepalli, S.Z. Nergiz, K.K. Liu, L. You, Y. Tang, S. Singamaneni, Y.S. Jun, Hydrophilic, Bactericidal nanoheater-enabled reverse osmosis membranes to improve fouling resistance, ACS Appl. Mater. Interfaces 7 (2015) 11117-11126.

[47] F. Foglia, S. Karan, M. Nania, Z. Jiang, A.E. Porter, R. Barker, A.G. Livingston, J.T. Cabral, Neutron reflectivity and performance of polyamide nanofilms for water desalination, Adv. Funct. Mater. 27 (2017) 1701738.

[48] G. Liu, W. Jin, N. Xu, Graphene-based membranes, Chem. Soc. Rev. 44 (2015) 5016-5030.

[49] Z. Chen, J. Wang, X. Duan, Y. Chu, X. Tan, S. Liu, S. Wang, Facile fabrication of 3D ferrous ion crosslinked graphene oxide hydrogel membranes for excellent water purification, Environ. Sci.: Nano 6 (2019) 3060-3071.

[50] M.R. Chowdhury, J. Steffes, B.D. Huey, J.R. McCutcheon, 3D printed polyamide membranes for desalination, Science 361 (2018) 682-686.

[51] Z. Jiang, S. Karan, A.G. Livingston, Water transport through ultrathin polyamide nanofilms used for reverse osmosis, Adv. Mater. 30 (2018) 1705973.

[52] N. Lan, K. Y. Wang, M. Weber, C. Maletzko, T. Chung, Investigation of novel molecularly tunable thin-film nanocomposite nanofiltration hollow fiber membranes for boron removal, J. Membr. Sci. 620 (2021) 118887.

[53] L. Bai, Y. Liu, N. Bossa, A. Ding, N. Ren, G. Li, H. Liang, M.R. Wiesner, Incorporation of cellulose nanocrystals (CNCs) into the polyamide layer of thin-film composite (TFC) nanofiltration membranes for enhanced separation performance and antifouling properties, Environ. Sci. Technol. 52 (2018) 11178-11187.

[54] Z. Yang, H. Guo, Z. Yao, Y. Mei, C. Tang, Hydrophilic silver nanoparticles induce selective nanochannels in thin film nanocomposite polyamide membranes, Environ. Sci. Technol. 53 (2019) 5301-5308.

[55] E.M. Van Wagner, A.C. Sagle, M.M. Sharma, B.D. Freeman, Effect of crossflow testing conditions, including feed pH and continuous feed filtration, on commercial reverse osmosis membrane performance, J. Membr. Sci. 345 (2009) 97-109.

[56] F. Xiao, X. Hu, Y. Chen, Y. Zhang, Porous Zr-based metal-organic frameworks (Zr-MOFs)-incorporated thin-film nanocomposite membrane toward enhanced desalination performance, ACS

Appl. Mater. Interfaces 11 (2019) 47390-47403.

[57] L.E. Peng, Z. Yao, Z. Yang, Guo, H.C.Y. Tang, Dissecting the role of substrate on the morphology and separation properties of thin film composite polyamide membranes: Seeing is believing, Environ. Sci. Technol. 54 (2020) 6978-6986.

[58] X. Kang, X. Liu, J. Liu, Y. Wen, J. Qi, X. Li, Spin-assisted interfacial polymerization strategy for graphene oxide-polyamide composite nanofiltration membrane with high performance, Appl. Surf. Sci. 508 (2020) 145198.

[59] R. Dai, J. Li, Z. Wang, Constructing interlayer to tailor structure and performance of thin-film composite polyamide membranes: A review, Adv. Colloid Interface Sci. 282 (2020) 102204.

[60] S. Zheng, Q. Tu, J.J. Urban, S. Li, B. Mi, Swelling of graphene oxide membranes in aqueous solution: Characterization of interlayer spacing and insight into water transport mechanisms, ACS Nano 11 (2017) 6440-6450.